This article has been accepted for publication in a future issue of this journal, but has not been fully edited. Content may change prior to final publication. Citation information: DOI 10.1109/TIE.2019.2901663, IEEE Transactions on Industrial Electronics

`

Improved Extended Kalman Filter Estimation using Threshold Signal Detection with a MEMS Electrostatic Micro-Scanner

Yi Chen, Haijun Li, Zhen Qiu, Thomas D. Wang, and Kenn R. Oldham

***Abstract*—A threshold signal detector is proposed to improve the state estimation accuracy of an extended Kalman filter (EKF) and is validated experimentally with a MEMS electrostatic micro-scanner. A first order derivative of Gaussian (DOG) filter is used to detect and locate rapid changes in voltage signal caused by crossing of a threshold angle determined by maximum overlap of capacitive electrodes. The event-triggered measurement is used in the update step of the EKF to provide intermittent but more accurate angle measurements than those of the capacitive sensor's continuous output. Experiments on the electrostatic micro-scanner show that with the threshold signal detector incorporated, the average position estimation accuracy of the EKF is improved by 15.1%, with largest improvement (30.3%) seen in low signal-to-noise ratio (SNR) conditions. A parametric study is conducted to examine sampling frequency and capacitance profile, among other factors that may affect detection error and EKF accuracy.**

***Index Terms*—Kalman filter, microsensors, signal processing.**

I. Introduction

Capacitive sensing technology, commonly used in microelectromechanical system (MEMS) devices, has advantages of low power operation, high sensitivity, and a relatively simple sensor structure compared to many other small-scale sensing mechanisms. The sensing principle is to measure the change of capacitance between two or more electrodes across a dielectric gap due to the change of gap geometry or the permittivity of the media between the gap. Various sensor geometries have been used in a vast array of sensing applications, such as measurement of short range distance (i.e. nano-positioning devices) [1], translational and rotational motion (i.e. MEMS inertial sensors) [2, 3], and pressure (i.e. microphone and pressure sensors) [4, 5].

One drawback of capacitive sensing is that its accuracy may be reduced by temperature and other environmental effects, which can cause undesired changes in geometric relations between electrodes [6] [7]. One potential solution is to find features of the sensing signal that correspond to specific positions that are both detectable and constant in the presence of unwanted geometric perturbations [8]. Such signal features can be used for measurement of threshold positions with high accuracy to "reset" position estimates and improve overall motion tracking accuracy. Design of capacitive sensors that generate threshold features can be intentional or a natural consequence of electrode geometry for a given application.

This paper introduces novel threshold signal detector realized with a derivative of Gaussian (DOG) function in the loop of an extended Kalman filter (EKF). It is intended to enhance angular position and velocity estimation for MEMS micro-scanners. The paper explores factors impacting the performance of the estimation scheme, such as noise level, capacitance profile of the sensor, sampling rate, etc.

Among prior research works, the idea of using threshold sensing to improve motion tracking can be found in Henningsson and Astrom's work [9], in which a sensor provided a measurement of the center mass of a MEMS accelerometer exceeding a threshold location; however, that literature did not discuss the realization of such a sensing mechanism. In [10], a design of an out-of-plane capacitive sensor using imbalanced capacitance to indicate threshold location was proposed; however, extraction of the signal was susceptible to drift of its capacitive signal. In [11], a Kalman filter estimation scheme with an asynchronized sensing scheme was proposed, in which a less accurate but frequently-measured analog signal and a highly accurate but infrequent (twice per period of a waveform) threshold signal were used in a Kalman filter estimator. That work, however, again did not address the issue of how to extract the threshold signal and assumed perfect detection. [8] proposed using a DOG filter to detect threshold crossing signals and embedded its output as a more accurate source of measurement updates within a Kalman filter estimator. However, experimental results were not presented, and issues such as sampling rate and how to fully incorporate a non-linear capacitive sensor model were not addressed.

Given the limitations of previous works, it is desirable to study factors that can affect the usage of threshold sensing in an EKF: how is the detection error distributed and can it be well-modelled by normal distributions? What is the relationship between the variance of error and factors including sensor design (capacitance profile) and operating conditions (sampling rate, noise)? How should one pick suitable parameters for the DOG filter to optimize EKF performance?

This work was partially supported in part by DARPA (Grant W31P4Q-12-1-0002), the National Institutes of Health (Grant 5-RQ1-EB-020644) and the National Science Foundation (Grant CMMI 1334340). (*Corresponding author: Yi Chen.*)

Y. Chen and K. R. Oldham are with the Department of Mechanical Engineering, University of Michigan, Ann Arbor, MI 48109, USA (e-mail: davidsky@umich.edu; oldham@umich.edu).

H. Li and T. D. Wang are with the Department of Biomedical Engineering, University of Michigan, Ann Arbor, MI 48109, USA (e-mail: haijunl@med.umich.edu; thomaswa@med.umich.edu).

Z. Qiu is with the Department of Biomedical Engineering, Michigan State University, East Lansing, MI, 48824, USA (e-mail: qiuzhen@msu.edu).

This article has been accepted for publication in a future issue of this journal, but has not been fully edited. Content may change prior to final publication. Citation information: DOI 10.1109/TIE.2019.2901663, IEEE Transactions on Industrial Electronics

The paper is structured as follows: Section II introduces some background on capacitive sensing, the DOG filter, and the EKF; Section III presents the process model, sensor model and EKF implementation; Section IV presents the experimental setup; Section V presents the results of parametric studies of factors that can impact estimator performance; Section VI presents experimental results; Section VII concludes the paper.

II. Preliminaries

A. Capacitive Sensing Principles

Most capacitive sensors rely on a change in the geometric relationship between two electrodes to measure displacement. The two most common approaches are to vary the electrode gap or vary their overlapped area [2]. In micro-scale devices, gap variation typically provides more sensitivity, at the cost of nonlinearity and a limited range of measurement. Change in area typically provides less sensitivity but more linear behavior, and may be designed to provide a unique feature of a maximal capacitance when electrodes reach their maximum overlapped area. We will examine a method to use such a geometric feature to generate and extract a threshold measurement that enhances accuracy of motion estimation by an EKF, and experimentally validate the method with a MEMS micro-scanner.

B. Electrostatic Micro-scanner and Threshold Sensing

The sample device studied in this paper, shown in Fig. 1 (a), is an electrostatically-driven dual-axis micro-scanner. It includes two reflective mirror surfaces for dual axes confocal imaging and multiple groups of comb-fingers. Each group of comb-fingers consists of a moveable comb and a fixed comb (Fig. 1 (b)). By applying driving voltage with a carefully selected frequency, the comb-finger can generate electrostatic torque that produces parametric resonance in the form of tilting motion with a frequency half that of the driving voltage [12].

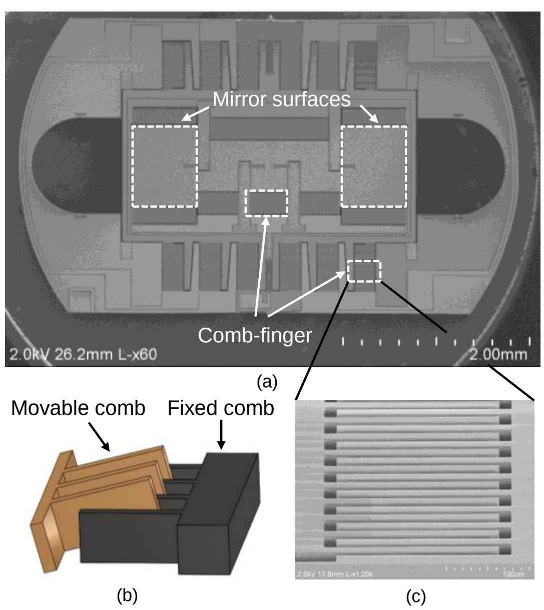

Fig. 1. (a) Scanning electron microscope image of a parametrically-resonant micro-scanner tested in this study. (a) Illustration of comb-finger electrodes used as actuators and capacitive sensors. (b) Zoomed in image of a representative comb-finger structure.

This class of micro-scanner is designed to deflect light for imaging purposes [13]. While the comb-fingers are designed to serve as actuators, they can also serve as capacitive sensors to measure the tilting angles of the mirror. The capacitance of the comb-finger as a function of tilting angle [14], is

$$C_s(\theta) = \frac{\epsilon_0 \epsilon_r n A(\theta)}{D} \tag{1}$$

where ε_r is the relative static permittivity (1 for air), ε_0 is the dielectric constant (8.8542 × 10-12 F m^{-1}), A is the overlap area of electrodes, D is the distance between the electrodes, $C_s(\theta)$ is sensing capacitance, $A(\theta)$ is the total area of overlap between the comb-fingers as a function of tilting angle θ, and n is the number of pairs of comb-fingers. The capacitance reaches its maximum when the overlapped area is maximized.

To transduce the capacitance change into measurable voltage signal, we employ a sensing circuit that applies constant bias voltage, V_{bias} at the sensing electrodes. The change of capacitance can be converted to a sensing current that is amplified by a feedback resistance, R_s, and trans-impedance amplifier into an analog voltage signal, y_{cap}, by

$$y_{cap} = -R_s V_{bias} \frac{dC_s(\theta)}{dt}. \tag{2}$$

It is worth noting that other types of sensing circuits can be applied [15]. Amplitude modulation and demodulation is commonly used to separate and suppress any feedthrough disturbance introduced by parasitic capacitance in the sensing electrodes coupling them to the device's driving voltage. However, modulation/demodulation also generates other effects including delays and skew in the filtered signal, which will can accuracy of a threshold measurement. In this study, since the focus is on validating the concept of generating and extracting threshold angle measurements and evaluating their effectiveness in an EKF framework, the transimpedance approach is used. This realization is also beneficial for implementation using very few electrical interconnects in a compact space, such as an endomicroscope. To compensate for feedthrough, later experiments were performed with a power cut-off strategy, discussed in section IV.

For this device, capacitance reaches its maximum value when the movable comb-fingers cross the mirror's central position and fully overlap the fixed comb-fingers. With the trans-impedance circuit, a rapid change in sign and magnitude of the output sensing signal occurs, as illustrated in Fig. 2 (a-d). This is referred to as the threshold angle for this system.

Knowing the exact timing of the threshold angle crossing is beneficial in high accuracy estimation of the angular position at that time. However, in practice it can be challenging to determine the threshold crossing time from the measured signal due to noise and bias. Since the threshold position crossing corresponds to a locally maximum rate of change of voltage, it might be obvious to adopt a derivative operator as a first attempt to retrieve crossing information. However, as illustrated in Fig. 2 (e), taking the derivative of a noisy signal does not necessarily provide a reliable outcome. To resolve this issue, a first order derivative of Gaussian (DOG) filter is proposed to extract the timing of the threshold position crossing [8]. A DOG filter is used as an approximated optimal filter for

This article has been accepted for publication in a future issue of this journal, but has not been fully edited. Content may change prior to final publication. Citation information: DOI 10.1109/TIE.2019.2901663, IEEE Transactions on Industrial Electronics

edge detection in the field of computer vision [16] and has merits of good detection (low probability of false detection), good localization (low variance of detection error), and one response to a single edge (one maximum or minimum corresponds to one crossing) [17].

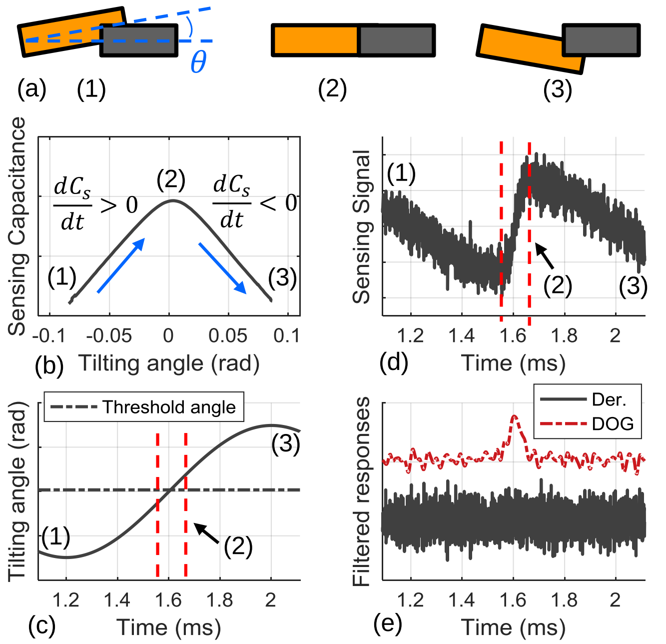

Fig. 2. An illustration of threshold angle crossing and mechanism of threshold angle sensing and detection. (a) Configurations of comb-finger (1), (2) and (3) correspond to before, at, and after threshold angle crossing. (b) Sensing capacitance vs. tilting angle θ. (c) Tilting angle vs. time. (d) Noisy sensing signal vs. time; the crossing event generates rapid change of signal around (2). (e) Comparison of filtered signal by a derivative operator and a DOG operator. DOG operator is effective in detecting the timing of rapid signal change.

While the introduction of a DOG filter provides an efficient and convenient realization for detecting threshold crossing timing, detection accuracy is still not perfect. In the presence of noise, the detected timing can deviate from the true timing. According to Canny [17], for the detection error in timing for a 1D step edge, $e_{t,th}$, its variance $R_{t,th}$ is expressed as

$$R_{t,th} = E\left[e_{t,th}^2\right] = \frac{\sigma_n^2 \int_{-W}^{W} \dot{f}(\tau)^2 d\tau}{\left[\int_{-W}^{W} \dot{f}(\tau)\dot{y}(-\tau) d\tau\right]^2} \tag{3}$$

where $f(\tau)$ is the filter for edge detection, $y(\tau)$ is the signal including the edge, τ is a dummy variable, and σ_n is the standard deviation of the normally distributed, zero mean additive noise to the sensing signal. This expression reveals that $R_{t,th}$ is proportional to the variance of noise (the noisier the signal, the less accurate the detection) and inversely proportional to the edge's slope (the sharper the slope, the more accurate the detection). $R_{t,th}$ is a key factor in threshold sensing performance and can be used to derive the error covariance matrix needed in to obtain optimal state estimates with an EKF.

C. Challenges

To carry out the EKF algorithm using threshold sensing information, a value for $R_{t,th}$ is needed. Although (3) gives a theoretical derivation, in operation, it is difficult to obtain a signal $y(t)$ containing an edge that is uncorrupted by noise. Hence it is desirable to estimate $R_{t,th}$ off-line, which leads to several issues. \First, the EKF assumes the process is subject to normally distributed noise. We will investigate the distribution of the $e_{t,th}$, and more importantly, the distribution of detection error of threshold angle, $e_{\theta,th}$, to ensure that the EKF can be appropriately applied. Second, the expression of $R_{t,th}$ in (3) is derived in continuous time and does not take sampling effects into account. Since the EKF is implemented in discrete time, choice of sampling rate can impact on estimation performance.

III. System Modelling

In this section, the process model, sensor model, and EKF incorporated with threshold sensing are described.

A. Process and Sensor Model

The dynamics of the tilting motion of the micro-scanner are modeled as a 2nd order, non-linear time invariant system.

$$J\ddot{\theta} + b_v\dot{\theta} + k_s\theta = \tau(\theta, V_{dr}) \tag{4}$$

where J is the moment of inertia of the micro-scanner, b_v is the damping coefficient, and k_s is the spring constant of a torsional spring. The torsional load generated by the comb-finger, τ_L is:

$$\tau_L(\theta, U) = \frac{1}{2}\frac{dC_{dr}}{d\theta}{V_{dr}}^2 \tag{5}$$

where V_{dr} is the driving voltage, and C_{dr} is the driving capacitance formed by the comb-fingers that generate tilting motion. Let $\boldsymbol{X} = [x_1\ x_2]^T$ to be state vector, where $x_1 = \theta$ and $x_2 = \dot{\theta} = \omega$ is the tilting angular velocity. Letting $\omega_n = \sqrt{k_s/J}$, $\zeta = \frac{b_v}{2\sqrt{Jk_s}}$, where ω_n is the natural frequency of the tilting mode and ζ is the damping ratio. (4) becomes:

$$\dot{\boldsymbol{X}} = \begin{bmatrix} 0 & 1 \\ -\omega_n^2 & -2\zeta\omega_n \end{bmatrix}\boldsymbol{X} + \frac{1}{2}\frac{dC_{dr}}{dx_1}{V_{dr}}^2 \tag{6}$$

Denoting the sampling interval to be T_s, and assuming that the process is subject to zero-mean, normally distributed process noise, the discretized process model for the EKF becomes

$$\boldsymbol{X}_k = g\left(\boldsymbol{X}_{\boldsymbol{k-1}}, V_{dr,k}\right) + \boldsymbol{v}_{\boldsymbol{k}} \tag{7}$$

where $g(\cdot)$ is defined as:

$$g\left(\boldsymbol{X}_{\boldsymbol{k-1}}, V_{dr,k}\right) = \begin{bmatrix} 1 & T_s \\ -\frac{k_s}{J}T_s & 1-\frac{b_v}{J}T_s \end{bmatrix}\boldsymbol{X}_{\boldsymbol{k-1}} + \begin{bmatrix} 0 \\ \frac{T_s}{2J} \end{bmatrix}\frac{dC_{dr}}{dx_1}(k){V_{dr,k}}^2 \tag{8}$$

For the sensor model, equation (2) shows that the signal from a capacitive sensor with current-based readout (Fig. 3 (c)) is proportional to the rate of change of capacitance, dC_s/dt. Since $\frac{dC_s}{dt} = \frac{dC_s}{d\theta}\frac{d\theta}{dt}$, where $\frac{dC_s}{d\theta}$ is the rate change of capacitance with respect to tilting angle θ. Denoting $\frac{d\theta}{dt} = \omega$, we have a measurement used by the EKF, y_{cap}, of:

$$y_{cap} = \left[-R_sV_{bias}\frac{dC_s}{d\theta}\right]\omega = h_{cap}(\theta)\omega \tag{9}$$

where $h_{cap}(\theta) = -R_sV_{bias}\frac{dC_s}{d\theta}$ is θ-dependent sensor gain, R_s is a constant resistance, and V_{bias} is a constant bias voltage.

This article has been accepted for publication in a future issue of this journal, but has not been fully edited. Content may change prior to final publication. Citation information: DOI 10.1109/TIE.2019.2901663, IEEE Transactions on Industrial Electronics

B. Extended Kalman Filter with Threshold Sensing

The proposed EKF includes a hybrid sensing scheme where the signal of the capacitive sensor is regarded as a normal analog measurement, and the detection of threshold crossing is applied intermittently. The procedure for applying the EKF with the fusion of the two types of measurements is provided in Table I. In Table I, $\boldsymbol{\hat{X}_k^-}$ is the *a priori* state estimates at the k-th step, $\boldsymbol{P_k^-}$ is the *a priori* error covariance matrix at the k-th step, $\boldsymbol{P_{k-1}}$ is the *a posteriori* error covariance matrix at the $(k-1)$-th step, $\boldsymbol{Q}$ is the covariance matrix of process noise, and $\boldsymbol{G_k} = \frac{\partial g}{\partial \boldsymbol{X_{k-1}}}$ is the Jacobian of the process model.

Depending on whether a threshold detection is positive, the form of the matrix of observation, $\boldsymbol{H_k}$, the estimated sensing signal, $\hat{Y}_k$ and the covariance matrix of measurement noise, $\boldsymbol{R}$, will vary. R_{cap} is the measurement noise variance for the

TABLE I

ALGORITHM, EKF WITH HYBRID SENSING SCHEME

1. Project *a priori* state estimates

$$\boldsymbol{\hat{X}_k^-} = g(\boldsymbol{\hat{X}_{k-1}}, V_{dr,k}); \quad \boldsymbol{P_k^-} = \boldsymbol{G_k P_{k-1} G_k^T} + \boldsymbol{Q}$$

2. Update matrix of observation

If threshold detection is negative

$$\boldsymbol{\hat{Y}_k} = [0\ h_{cap}(\hat{\theta}_k^-)]\boldsymbol{\hat{X}_k^-} = \boldsymbol{H_k \hat{X}_k^-}; \quad \boldsymbol{R} = R_{cap}$$

If threshold detection is positive

$$\boldsymbol{\hat{Y}}_k = \begin{bmatrix} 1 & 0 \\ 0 & h_{cap}(\hat{\theta}_k^-) \end{bmatrix} \boldsymbol{\hat{X}_k^-} = \boldsymbol{H_k \hat{X}_k^-}; \quad \boldsymbol{R} = \begin{bmatrix} R_{\theta,th} & 0 \\ 0 & R_{cap} \end{bmatrix}$$

3. Compute EKF gain with threshold sensing

$$\boldsymbol{K}_k = \boldsymbol{P_k^- H_k^T}\left(\boldsymbol{H_k P_k^- H_k^T} + \boldsymbol{R}\right)^{-1}$$

4. Update *a posteriori* state estimates

$$\boldsymbol{\hat{X}_k} = \boldsymbol{\hat{X}_k^-} + \boldsymbol{K_k}\left(\boldsymbol{Y_k} - \boldsymbol{\hat{Y}_k}\right); \quad \boldsymbol{P_k} = \boldsymbol{P_k^-} - \boldsymbol{K_k H_k^T P_k^-}$$

analog capacitance signal and $R_{\theta,th}$ is the variance of $e_{\theta,th}$. The Kalman gain $\boldsymbol{K_k}$ is then computed and *a posteriori* state estimates $\boldsymbol{\hat{X}_k}$ and *a posteriori* estimate error covariance matrix P_k are finally updated with the measurement at the k-th step, Y_k. Measurement $\boldsymbol{Y_k} = \left[\theta_{th}\ \ y_{cap,k}\right]^T$ for positive detection and $\boldsymbol{Y_k} = y_{cap,k}$ for negative detection.

IV. EXPERIMENTS AND MODEL IDENTIFICATION

An experimental testbed was prepared and used to identify parameters of the process and sensor models, and to verify the effectiveness of the DOG filter in threshold crossing detection and the EKF using the hybrid sensing scheme.

A. Experimental Set-up and Methods

As depicted in Fig. 3(a), computer-generated voltage commands were transmitted to an NI PCIe 6251 DAQ with sampling rate of 500 kHz. The voltage command was amplified by a TEGAM 2340 amplifier with 20 times amplification, and the amplified driving voltage fed to the MEMS scanner to generate tilting motions. Tilting motion was measured by two means: reflection of a laser by the scanner and conversion of the capacitive sensing current as described in equation (9).

Laser tracking is treated as the ground truth of tilting motion. Fig. 3 (b) shows the geometric relation between the MEMS scanner mounted on a dual inline package, a JDSU 1500 helium-neon laser source, and an On-Trak 1L10 position sensing detector (PSD). The laser beam is emitted by the source, reflected by the scanner's mirror surface, and received by the PSD, amplified by an On-Trak-301SL sensing amplifier.

On-chip sensing is used by the EKF. Fig. 3 (c) depicts the schematic of integrated driving and sensing circuitry. An AC driving voltage is fed into comb-fingers used for driving, and a DC bias voltage provided by a source meter, V_{bias}, is fed into comb-fingers used for sensing. The generated current flow through the shared grounding terminal is fed into a sensing circuit, which consists of a TI OPA2140 amplifier with a feedback resistance of 10 Mohm.

Since the objective of the study is to validate the method of using a DOG filter for threshold angle crossing detection and EKF integration, it is useful to eliminate potential disturbances introduced by feedthrough of the driving voltage. Therefore, during experiments, a power cut-off method was applied. A

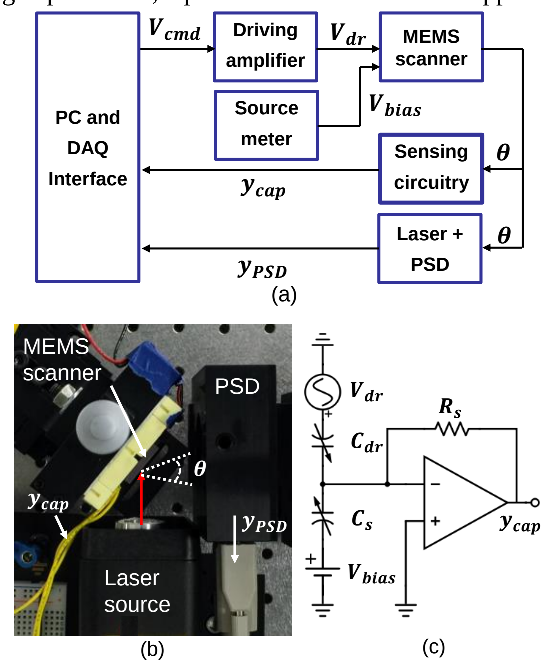

Fig. 3. Experimental set-up: (a) Schematic of major experimental modules and signal flow. (b) Top view of set-up and illustration of geometric relationship between the laser source, MEMS scanner and PSD. (c) Schematic sensing and driving circuitry for the MEMS scanner.

Zero to 60 volt periodic V_{dr} was applied to the MEMS scanner, and the frequency was swept from 1600 Hz to 1220 Hz to reach a maximized amplitude of tilting motion given electrostatic spring softening [18]. Once the tilting motion was stabilized, V_{dr} was set to zero, while V_{bias} was maintained at a constant 10 volts. Such a sequence of voltage commands allows the micro-scanner to freely oscillate briefly after the power cut-off, and the sensing current induced by the oscillation can be amplified and recorded without feedthrough disturbance.

A total 10 trials of power cut-off experiments were performed and the V_{dr}, y_{cap} and y_{PSD} were recorded at 500 kHz rate. The data was post-processed as follows for consistency: Each time series was truncated at the power cut-off and 80 ms afterwards (approximately 50 periods of free oscillation). The delay between PSD measurement and sensing circuit measurement was experimentally calibrated to be 0.114 ms.

This article has been accepted for publication in a future issue of this journal, but has not been fully edited. Content may change prior to final publication. Citation information: DOI 10.1109/TIE.2019.2901663, IEEE Transactions on Industrial Electronics

`

To detect a threshold crossing, a DOG filter is applied to the sensing signal using the *nlfilter* function in MATLAB, which is a general sliding-neighborhood operation. The filtered signal is then processed with non-maximum suppression to suppress the filtered response except the local maxima, and these local maxima are then extracted to indicate the detected threshold crossing. In this study, the threshold detections are extracted in a post-processing fashion. To achieve a near real-time threshold detection, a buffer can be used to store measurements from past to present, and DOG filter can be applied to the signal in the buffer to generate a local maximum for threshold detection.

B. Identification of Process and Sensor Models

The tilting angle measured by the PSD, θ_{PSD} is computed as

$$\theta_{PSD} = \arctan(\frac{y_{PSD}G_{PSD}}{L_m}) \tag{10}$$

where G_{PSD}(0.5 mm/V) is the gain of the PSD sensing amplifier and L_m is the distance from the scanner surface to PSD surface

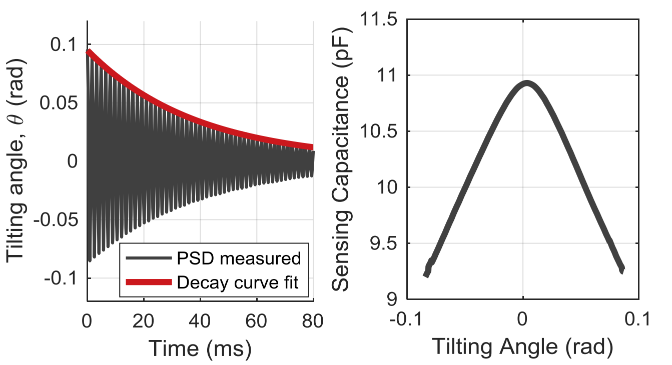

(a) (b)

Fig. 4. (a) Experimentally measured free oscillations vs. simulated decay curve of free oscillations with identified natural frequency and damping ratio of the MEMS scanner. (b) Experimentally identified sensing capacitance with respect to tilting angle.

TABLE II
BASE SETTING FOR PARAMETRIC STUDY

Symbol	Description	Value
f_s	sampling frequency	500 kHz
θ_{amp}	amplitude of θ	0.15 rad
f_m	motion frequency	625 Hz
σ_n	standard deviation of noise	0.0435 V
R_s	feedback resistance	10 MΩ
V_{bias}	bias voltage	10 V
w_{DOG}	width of DOG filter	400
σ_{DOG}	standard deviation of DOG filter	15

and is measured to be 32.7 mm. A representative trajectory of the system is shown Fig. 4 (a); by fitting the decay curve using linear viscous damping [19], ω_n and ζ were identified to be 624.6 Hz and 0.0066, respectively.

The sensor model is the sensing capacitance as a non-linear function of angle, $C_s(\theta)$, which can be experimentally identified by mapping the trajectory $C_s(t)$ versus $\theta_{PSD}(t)$ in various experiments. First, $C_s(t)$ is obtained by integrating y_{cap} with respect to time, from (2):

$$C_s(t) = \int_{t_0}^{t_f} -R_s V_{bias} y_{cap} dt \tag{11}$$

Using the corresponding $\theta_{PSD}(t)$ one can establish a mapping of $C_s(\theta)$ and $\frac{dC_s}{d\theta}(\theta)$ and therefore compute $h_{cap}(\theta)$ as suggested in equation (9). Fig. 4 (b) shows the identified sensor gain function $h_{cap}(\theta)$. The capacitance profile can be approximated by a Gaussian model [14].

The threshold location, θ_{th} is identified by computing the average angular displacement at which the peak capacitance is reached among the experimental measurements. Nominally, θ_{th} should be zero for the planar micro-scanner geometry, but in practice a non-zero value may occur due to finite fabrication tolerance of electrodes and residual stresses. In this device θ_{th} was calibrated to be 0.0037 rad.

V. PARAMETRIC STUDY OF FACTORS IMPACTING THRESHOLD DETECTION

In this section, parametric studies investigate the properties of the error of threshold detection and some contributing factors, including the sensor map and sampling rate. A sinusoidal tilting motion is simulated within the capacitive sensor model described by (9), with additive, zero-mean normally distributed measurement noise. The signal generated by the capacitive sensing model is passed into a DOG filter to compute the detection error in timing $e_{t,th}$ and detection error in threshold angle $e_{\theta,th}$. Baseline settings from experimental device identification are summarized in Table II.

A. Sampling Rate Effects

In (3), sampling rate is not singled out as a factor that affects the detection of threshold signal. However, this is not the case during digital implementation, as a low sampling rate introduces quantization error and a high sampling rate may allow excessive sensor noise into the filtering process. Therefore a series of simulations was conducted, from the baseline in Table II, and the sampling rate was swept from 50 kHz to 5 MHz. The filter size was adjusted proportionally to maintain a fixed ratio between the filter size and the period of the waveform. The signal-to-noise ratio (SNR) was also varied by multiplying σ_n by factors of 0.1 and 10.

The simulation result is shown in Fig. 5 (a). The result shows that $R_{t,th}$ increases as sampling rate is slower than 1250 kHz, mainly due to quantization noise. As the sampling rate increases, $R_{t,th}$ increases, attributed to noisier samples being taken into the filtering process. This suggest that an optimal selection for sampling frequency for a given threshold sensor exists, and one can properly size the data acquisition system to achieve the lowest variance of detection timing error without overreaching for fast sampling capability.

B. Sensor Map Effects

Equation (3) suggests that the variance of detection timing error is inversely proportional to the rate of change of the signal $\dot{y}(t)$, meaning that a sharper and more abrupt change of signal amplitude can be more accurately located in a statistical sense. To test the significance of the change, one way is to change of the capacitance profile formed by the electrodes. More specifically, we are interested in $dC_s/d\theta$ around threshold location, as higher values will prompt higher $\dot{y}_{cap}(t)$ as

This article has been accepted for publication in a future issue of this journal, but has not been fully edited. Content may change prior to final publication. Citation information: DOI 10.1109/TIE.2019.2901663, IEEE Transactions on Industrial Electronics

suggested in (9). In this study, a modified logistic function is used to generate a modelled sensor gain, $\hat{h}_{cap}$ as:

$$\hat{h}_{cap}(\theta) = N_g\left(\frac{1}{1+e^{-N_\theta \theta}} - 0.5\right) \qquad (12)$$

where N_g is the normalization factor for gain, and N_θ is the normalization factor for angle. The modelled sensing capacitance simply takes the integration of $\hat{h}_{cap}(\theta)$ with

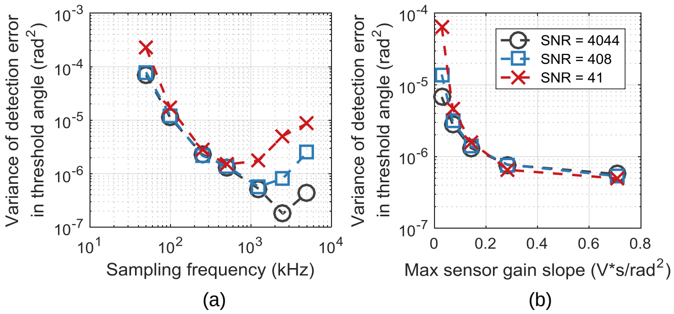

Fig. 5. (a) Variance of detection error in threshold angle vs. sampling frequency. (b) Variance of detection error in threshold angle vs. maximum sensor gain slope.

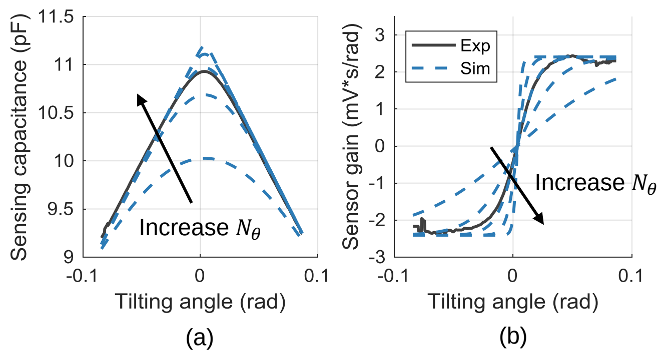

Fig. 6. Sweep of maximum sensor gain slope. (a) Sensing capacitance becomes sharper around threshold angle as N_θ increase. (b) Sensor gain slope becomes steeper around threshold angle as N_θ increases.

respect to tilting angle:

$$\hat{C}_s(\theta) = -\frac{1}{R_s V_{bias}}\int_{\theta_{min}}^{\theta_{max}} \hat{h}_{cap}(\theta)\, d\theta \qquad (13)$$

By sweeping N_θ one can vary the maximum sensor gain at the vicinity of threshold location, with larger N_θ corresponding to steeper slop and more drastic change of capacitance at θ_{th}, as depicted in Fig. 6. The experimentally identified sensor gain was used as baseline to generate a series of sensor model with N_θ swept from 0.2 to 5.

Fig. 5 (b) shows the simulation results. We find that $R_{t,th}$ decreases as expected as the maximum sensor gain slope increases. The significance of this change is comparable at various sensor noise densities.

VI. Experimental Results

In this section, experimental results are presented to evaluate the effect of different DOG filters on threshold detection and EKF performance. The decaying tilting motion of the micro-scanner after power cut-off provides an opportunity to vary SNR by segmenting trajectories. Therefore, for each trial the measurements and estimated states are divided into 4 segments, with SNR ranging from 85 to 1. For conciseness, the EKF using the hybrid sensing scheme of capacitive analog sensing and threshold sensing is abbreviated as HYB.

A. Effect of DOG Filter on Threshold Detection

The EKF implementation assumes that process noise and measurement noise are normally distributed. Therefore, it is helpful to verify the distribution of measurement noise of the threshold sensor. Threshold angle measurement noise is defined as the error between the threshold angle and the ground truth angle at the instant of detection, denoted as $e_{\theta,th}$. Here, $e_{t,th}$ and $e_{\theta,th}$ are computed by taking the differences between the timing and angle at the detected threshold crossing and their ground truth values, respectively. The distribution of $e_{t,th}$and $e_{\theta,th}$ computed from experimental measurements was analyzed using the Kolmogorov-Smirnov test [20]. Results indicate that the error distribution can be well-modeled by normal distributions at the tested conditions, shown in Fig. 7.

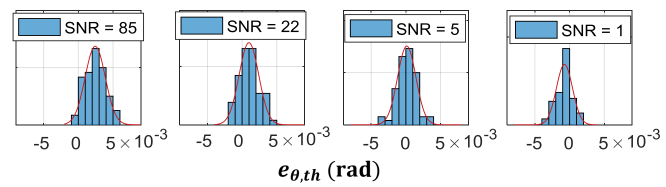

Fig. 7. Distribution of detection errors in threshold angle from experimental measurements at different signal-to-noise ratios can be well modeled by normal distributions.

Different settings for the DOG filter were also applied to y_{cap} and the EKF to evaluate their impact on the variance of $e_{\theta,th}$and accuracy of state estimation. The filter size w_{DOG} was swept from 80 sample points to 400 sample points and σ_{DOG} was swept from 1.5 to 45. No significant performance variation was found in varying w_{DOG} while keeping σ_{DOG} the same. However, as shown in Fig. 8, the variance of $e_{\theta,th}$ varies as σ_{DOG} varies for all four cases, which suggests a large σ_{DOG} is beneficial in reducing overall error variance.

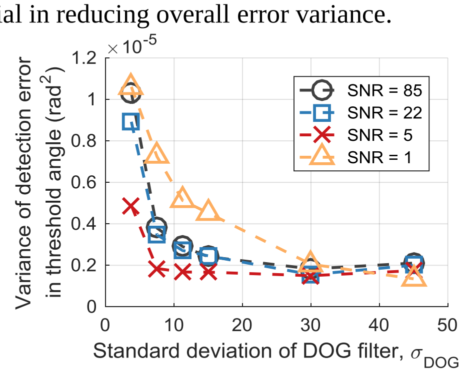

Fig. 8. Variance of detection error in threshold angle during experiments with respect to the standard deviation of DOG filter.

B. Effect of Threshold Sensing on EKF

A representative estimation result is depicted in Fig. 9. The ground truth (EXP) and estimated tilting motion (EKF and HYB) are shown.

This article has been accepted for publication in a future issue of this journal, but has not been fully edited. Content may change prior to final publication. Citation information: DOI 10.1109/TIE.2019.2901663, IEEE Transactions on Industrial Electronics

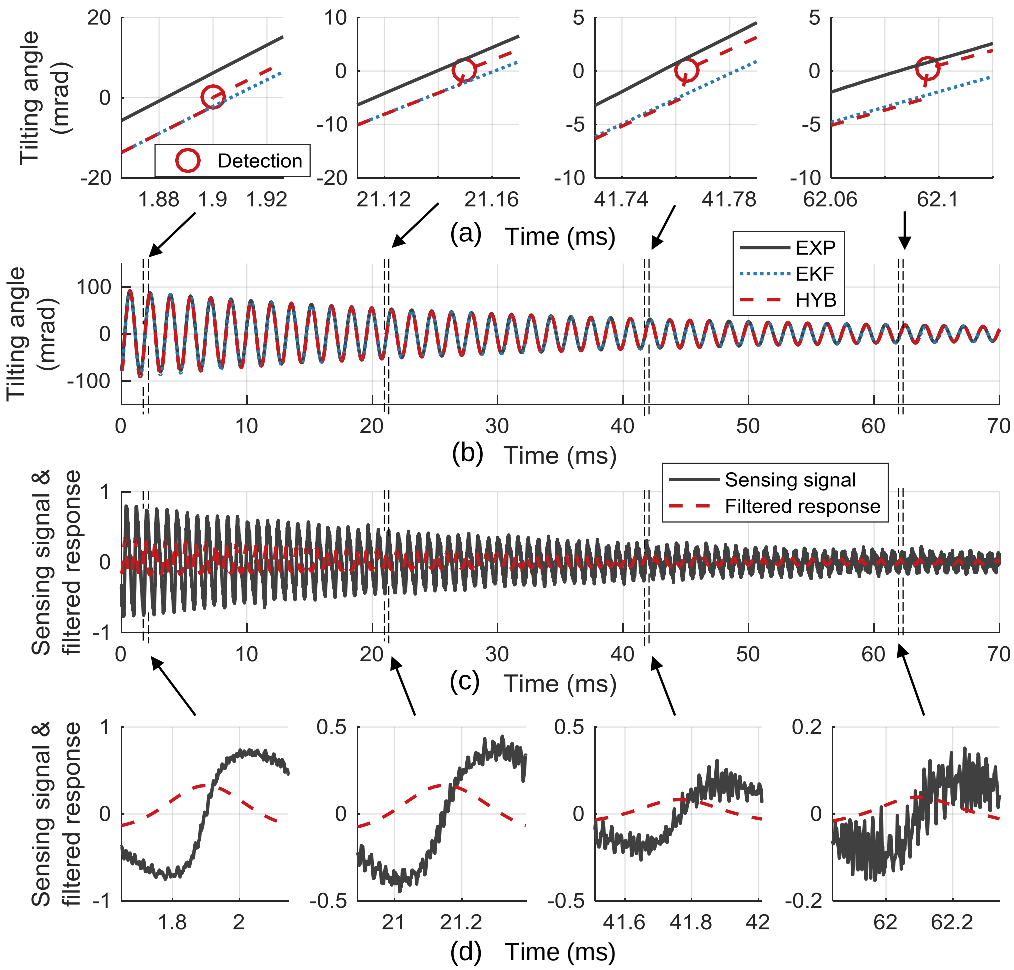

Fig. 9. A representative experimental measurement and estimation result in time domain. (a) Four snapshots of threshold angle crossing detection improving tilting angle estimation. (b) Overall trajectories of tilting angle measurement and estimations. (c) Overall trajectories of sensing signal and response of DOG filter. (d) Corresponding snapshots of sensing signal, where local maxima of filtered response detects threshold angle crossing.

Fig. 9 (a) shows the change in estimator output with introduction of threshold crossing detection: $\hat{\theta}$ by HYB is corrected at the instant of threshold crossing detection and therefore is closer to the ground truth value. Fig. 9 (d) shows that the local maxima of the DOG filter response corresponds to the vicinity of the maximal rate of change of y_{cap} and serves as a detection of threshold angle crossing. The four snapshots demonstrate that the detection method is robust under various SNR conditions.

Root mean square error (RMSE) of tilting angle θ_{RMSE} is defined as a performance metric:

$$\theta_{RMSE} = \sqrt{\frac{1}{N}\sum_{i=1}^{N}\left(\hat{\theta}_i - \theta_{PSD,i}\right)^2} \tag{14}$$

where $\widehat{\theta_i}$ is *a posteriori* estimate of tilting angle and $\theta_{PSD,i}$ is the tilting angle measured by the PSD at the i-th sampling instance, and N is the number of sampling instants. A normalized root mean square error (NRMSE) of tilting angle, θ_{NRMSE} is also defined and examined:

$$\theta_{NRMSE} = \frac{\theta_{RMSE}}{\bar{\theta}_{amp}} \tag{15}$$

where $\bar{\theta}_{amp}$ is the average amplitude of the corresponding waveforms. θ_{RMSE} and θ_{NRMSE} are evaluated for the overall trajectories as well as each segment.

To evaluate the improvement made by introducing threshold

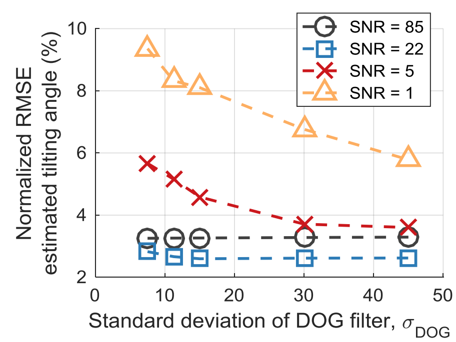

Fig. 10. Normalized RMSE with different signal-to-noise ratios and various σ_{DOG} settings. Under noisy condition (low SNR), increasing σ_{DoG} effectively increases threshold detection accuracy and therefore increases state estimation accuracy of the EKF.

This article has been accepted for publication in a future issue of this journal, but has not been fully edited. Content may change prior to final publication. Citation information: DOI 10.1109/TIE.2019.2901663, IEEE Transactions on Industrial Electronics

TABLE III

SUMMARY OF RMSE OF ESTIMATED TILTING ANGLE

	SNR 85	SNR 22	SNR 5	SNR 1	Overall
EKF θ_{RMSE}	0.0050	0.0029	0.0026	0.0025	0.0034
HYB θ_{RMSE}	0.0047	0.0023	0.0019	0.0018	0.0029
$\boldsymbol{\theta_{RMSE}}$ reduced	**6.9%**	**21.4%**	**27.6%**	**30.3%**	**15.1%**
EKF $\theta_{RMSE,th}$	0.0055	0.0051	0.0050	0.0049	0.0051
HYB $\theta_{RMSE,th}$	0.0041	0.0045	0.0049	0.0045	0.0045
$\boldsymbol{\theta_{RME,th}}$ reduced	**26.0%**	**11.6%**	**2.6%**	**8.1%**	**12.3%**

sensing to the EKF, the θ_{RMSE} within each segment of estimation trajectory generated by the two estimators are computed. Here $\theta_{RMSE,th}$ denotes the RMSE computed using 50 sample points after each threshold detection occurred. The results are listed in Table III.

From Table III we can see that the largest percentage improvement of total RMSE happens with SNR = 1. The largest improvement of RMSE after threshold detection location happens with SNR = 85. The result shows that the threshold sensing adds the greatest local accuracy in high SNR conditions, but is more beneficial for overall EKF performance when SNR is low.

The trend of θ_{NRMSE} of each segment with respect to different σ_{DOG} is shown in Fig. 10. For segments with high SNR (85 and 22), the change of σ_{DOG} does not significantly change θ_{NRMSE}. However, for segments with low SNR (5 and 1), the analysis shows increasing σ_{DOG} significantly reduces θ_{NRMSE}, which suggests that the performance of EKF with threshold sensing is sensitive to selection of σ_{DOG}.

I. CONCLUSION

We introduce a method for utilizing a first order derivative of Gaussian (DOG) operator to detect threshold crossing from noisy signal and integrated this detection mechanism into an EKF to estimate states from a non-linear process. To verify the effectiveness of the method, experimental and simulation studies have been conducted to estimate the tilting angle of an electrostatic micro-scanner, and quantify various factors that might affect the error of threshold detection and EKF performance. Simulation shows: (1) an optimal sampling frequency exists for a minimal variance of detection timing error; (2) increasing $G_{cap}(\theta)$ around threshold angle reduces variance of detection error in timing and angle, beneficial for improving EKF accuracy.

Experimental results show that use of the threshold sensing mechanism improved EKF performance across SNR conditions on a MEMS micro-scanner, with best improvement of a 30.3% reduction in RMSE of tilting angle estimation. On average, using threshold sensing improves the RMSE by 15.1% across a range of SNR scenarios. A sweep of width σ_{DOG} of the DOG filter also shows that for low SNR, threshold detection accuracy is more sensitive to DOG filter parameter such as σ_{DOG} and therefore needs to be selected carefully to so that EKF can maximize the performance improvement of using the DOG filter.

ACKNOWLEDGMENT

The authors would like to thank Mayur Birla for his help in taking SEM images of the device.

REFERENCES

[1] A. J. Fleming, "A review of nanometer resolution position sensors: Operation and performance," *Sensors and Actuators A: Physical,* vol. 190, no. 1, pp. 106 - 126, 2013.

[2] D. K. Shaeffer, "MEMS inertial sensors: a tutorial overview," *IEEE Communications Magazine,* pp. 100 - 109, 11 April 2013.

[3] Y. Chen, E. E. Aktakka, J.-K. Woo, K. Najafi and K. R. Oldham, "On-chip capacitive sensing and tilting motion estimation of a micro-stage for in situ MEMS gyroscope calibration," *Mechatronics,* 2018.

[4] P. R. Scheeper, A. v. d. Donk, W. Olthuis and P. Bergveld, "A review of silicon microphones," *Sensors and actuators A: Physical,* vol. 44, no. 1, pp. 1 - 11, 1994.

[5] W. P. Eaton and J. H. Smith, "Micromachined pressure sensors: review and recent developments," *Smart Materials and Structures,* vol. 6, no. 5, p. 530, 1997.

[6] C. Acar and A. Shkel, MEMS vibratory gyroscopes: structural approaches to improve robustness, Springer Science & Business Media, 2008.

[7] G. Stemme, "Resonant silicon sensors," *Journal of Micromechanics and Microengineering,* vol. 1, no. 2, p. 113, 1991.

[8] Y. Chen and K. R. Oldham, "Kalman filter estimation with edge detection-based hybrid sensing," in *American control Conference*, Boston, 2016.

[9] T. Henningsson and K. J. Åström, "Log-concave observers," in *Proc. of Mathematical Theory of Networks and Systems*, Kyoto, 2006.

[10] Y. Chen, E. E. Aktakka, J.-K. Woo and K. Oldham, "Threshold sensing signal construction from a capacitive sensor for MEMS gyroscope calibration," in *IEEE International Conference on Advanced Intelligent Mechatronics (AIM),* Banff, 2016.

[11] B. Edamana, Y. Chen, D. Slavin, E. E. Akatakka and K. R. Oldham, "Estimation with threshold sensing for gyroscope calibration using a piezoelectric microstage," *IEEE Transactions on Control Systems Technology,* vol. 23, no. 5, pp. 1943 - 1951, 2015.

[12] H. Schenk, P. Dürr, T. Haase, D. Kunze, U. Sobe, H. Lakner and H. Kück, "Large deflection micromechanical scanning mirrors for linear scans and pattern generation," *IEEE Journal of Selected Topics in Quantum Electronics,* vol. 6, no. 5, pp. 715 - 722, 2000.

[13] H. Li, X. Duan, Z. Qiu, Q. Zhou, K. Kurabayashi, K. R. Oldham and T. D. Wang, "Integrated monolithic 3D MEMS scanner for switchable real time vertical/horizontal cross-sectional imaging," *Optics Express,* vol. 24, no. 3, pp. 2145-2155, 2016.

[14] W. Shahid, Z. Qiu, X. Duan, L. Haijun, T. D. Wang and R. K. Oldham, "Modeling and Simulation of a Parametrically Resonant Micromirror With Duty-Cycled Excitation," *Journal of Microelectromechanical Systems,* pp. 1440 - 1453, 2014.

[15] N. Yazdi, H. Kulah and K. Najafi, "Precision readout circuits for capacitive microaccelerometers," in *Proceedings of IEEE Sensors 2004,* Vienna, 2004.

[16] M. Basu, "Gaussian-based edge-detection methods-a survey," *IEEE Transactions on Systems, Man, and Cybernetics, Part C (Applications and Reviews),* vol. 32, no. 3, pp. 252 - 260, 2002.

[17] J. Canny, "A computational approach to edge detection," *IEEE Transactions on pattern analysis and machine intelligence 6,* pp. 679 - 698, 1986.

[18] S. T. Holmstrom, U. Baran and H. Urey, "MEMS Laser Scanners: A Review," *Journal of Microelectromechanical Systems,* vol. 23, no. 2, pp. 259 - 275, 2014.

[19] M. R. K. J. T. S. Richard Schroedter, "Flatness-based open-loop and closed-loop control for electrostatic quasi-static microscanners using jerk-limited trajectory design," *Mechatronics,* 2017.

[20] H. W. Lilliefors, "On the Kolmogorov-Smirnov Test for Normality with Mean and Variance Unknown," *Journal of the American statistical Association,* vol. 62, no. 318, pp. 399-402, 1967.

[21] S. Thrun, W. Burgard and F. Dieter, Probabilistic robotics, London:

The MIT Press, 2005.

[22] U. Hofmann, J. Janes and H.-J. Quenzer, "High-Q MEMS resonators for laser beam scanning displays," *Micromachines,* vol. 3, no. 2, pp. 509 - 528, 2012.

Yi Chen received the B.S. degrees in mechanical engineering from the University of Michigan and Shanghai Jiao Tong University in 2010. He received two Master's degrees in mechanical engineering and electrical engineering and a Ph.D. degree in mechanical engineering from the University of Michigan in 2012, 2018 respectively.

He is currently an software engineer with Midea Emerging Technology Center. His research interests include computer vision and robotics.

Haijun Li received the Ph.D. degree in microelectronics and solid-state electronics from Jilin University, Changchun, China, in 2007. He held a post-doctoral position at Nanyang Technology University, Singapore, from 2008 to 2011. He was a Senior Engineer at the Hebei Semiconductor Research Institute, Shijiazhuang, China, from 1997 to 2008.

He is currently a Research Investigator with the University of Michigan, Ann Arbor, MI, USA, where he is involved in the development of MEMS-based endomicroscope. His research interests include MEMS, uncooled infrared detectors, epi-MEMS technology, and wafer level packaging technologies.

Zhen Qiu was born in Wuhu, Anhui, China. He received the Bachelor Degree in the Department of Precision Instruments, Tsinghua University, Beijing, China, and the Ph.D. degree from the Department of Biomedical Engineering, University of Michigan-Ann Arbor, MI, USA, in 2004, 2013, respectively.

He finished his post-doctoral training in the Department of Radiology and Molecular Imaging Program Stanford (MIPS), School of Medicine, Stanford University, CA. He is currently an Assistant Professor in the Department of Biomedical Engineering, Institute for Quantitative Health Science and Engineering, Michigan State University, MI. His research interests include biomedical optics, MEMS/MOEMS, multi-modal targeted imaging using novel contrast agents, wearable and implantable medical devices, ultrafast laser applications.

Professor Qiu is currently holding the member of SPIE and OSA.

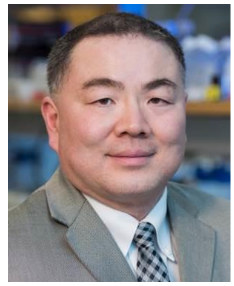

Thomas D. Wang received his B.S. degree in Mathematics and Physics from Harvey Mudd College and Ph.D. degree in medical engineering and medical physics from MIT.

He is currently a Professor of Medicine, Biomedical Engineering, and Mechanical Engineering at the University of Michigan and the H. Marvin Pollard Collegiate Professor of Endoscopy Research. His research interests are in the field of biomedical optics, multiplexed detection, and molecular imaging. He has developed a number of microsystems-based technologies to perform scanning and actuation for high speed imaging with large working distance in endomicroscopy.

Kenn R. Oldham received the Ph.D. in Mechanical Engineering from the University of California at Berkeley in 2006 and the B.S. in Mechanical Engineering from Carnegie Mellon University in 2000. He is currently an Associate Professor of Mechanical Engineering at the University of Michigan. His research focuses on the intersection of control systems and micro-scale sensing and actuation, with interests in design for controllability, optimal and robust control, microsystem estimation and identification, and novel sensor and actuator design. Applications include terrestrial micro-robotics, endoscopic microscopy, and inertial and physiological sensing.